Marine Geology
November 2007, Volume 246, Issue 1, Pages 42-59
http://dx.doi.org/10.1016/j.margeo.2007.08.002

High resolution seafloor images in the Gulf of Cadiz, Iberian margin

V. Hanquiez[1, *], T. Mulder[1], P. Lecroart[1], E. Gonthier[1], E. Marchès[1], M. Voisset[2]

[1]Université Bordeaux 1; CNRS; UMR 5805-EPOC, avenue des facultés Talence, 33405 France.
[2]IFREMER; Département Géosciences Marines, BP 70, Plouzané, 29280 France.

*: Corresponding author : Hanquiez V., email address : v.hanquiez@epoc.u-bordeaux1.fr, Tel: 33 5 40 00 34 35. Fax: 33 55 68 84 08 48.

Abstract:

In the Gulf of Cadiz, the hydrodynamic process acting on particle transport and deposition is a strong density-driven bottom current caused by the outflow of the saline deep Mediterranean water at the Strait of Gibraltar: the Mediterranean Outflow Water (MOW). New high resolution acoustic data including EM300 multibeam echo-sounder, deep-towed acoustic system SAR and very high resolution seismic, completed by piston cores collected during the CADISAR cruise allow to improve the understanding of the hydrodynamics of the MOW in the eastern part of the Gulf of Cadiz. Interpretation of data corrects the previous model established in this area and allows, for the first time, the accurate characterization of various bedforms and erosive structures along the MOW pathway and the precise identification of numerous gravity instabilities. The interaction between the MOW, the seafloor morphology and the Coriolis force is presently the driving force of the sedimentary distribution pattern observed on the Gulf of Cadiz continental slope.

Keywords: Gulf of Cadiz; Mediterranean Outflow Water (MOW); Contourites; deep-towed SAR; acoustic facies; sedimentary processes; instabilities

1. Introduction

The Gulf of Cadiz is located between the Strait of Gibraltar (Spain) and the Cape St Vincent (Portugal). The Gulf is placed at the Eurasian and African plate boundary and subjected to complex tectonic processes (Srivastava et al., 1990; Sartori et al., 1994; Maldonado and Nelson, 1999). This tectonic activity is partly responsible for the formation of the diapiric ridges diverting the Mediterranean Outflow Water (MOW) pathway since the Quaternary (Nelson et al., 1993; Llave et al., 2007).

Present day water circulation along the Gulf of Cadiz margin is controlled by the exchanges between the Atlantic Inflow surface current circulating as deep as 300 m (Mélières, 1974), and the MOW bottom current flowing between 300 and 1500 m water depth (Madelain, 1970; Ambar et al., 1999) (Figure 1). The MOW flows westward just west of the strait of Gibraltar with a velocity reaching 2.5 m s-1 (Boyum, 1967; Madelain, 1970; Ambar and Howe, 1979). West of 6°20'W, the MOW is deflected northward and splits into two cores (Madelain, 1970; Zenk, 1975; Ambar and Howe,1979; Gardner and Kidd, 1983; Ochoa and Bray, 1991; Johnson and Stevens, 2000; Borenäs et al., 2002; García, 2002; Hernández-Molina et al., 2003): (1) the Mediterranean Upper Water (MUW, Figure 1), a geostrophic current following a northerly path between 300 and 600 m water depth (Ambar and Howe, 1979; Ambar et al., 1999; Baringer and Price, 1999), and (2) the Mediterranean Lower Water (MLW, Figure 1), an ageostrophic current flowing westwardly from the Strait of Gibraltar, at water depths ranging from 600 to 1500 m (Madelain, 1970; Zenk and Armi, 1990; Baringer, 1993; Bower et al., 1997). At about 7°W, the MLW splits into three branches (Intermediate/IMB, Principal/PMB and Southern/SMB; Madelain, 1970; Kenyon and

Belderson, 1973; Mélières, 1974; Nelson et al., 1993; García, 2002), due to a complex bathymetry (Figure 2) previously described by Mulder et al. (2003) and Hernández-Molina et al. (2003, 2006). According to the distribution of Hernández-Molina et al. (2003), three morpho-sedimentary sectors are distinguished in this area:

(1) The proximal scour and sand-ribbons sector with the Main MOW Channel (MMC, Figure 2) which drains the MUW and the MLW.

(2) The channels and ridges sector with (i) the Cadiz Contourite Channel (CC, Figure 2) which drains the SMB, the Huelva Channel (HC, Figure 2) which drains the IMB, and the Guadalquivir Channel (GC, Figure 2) which drains the PMB; (ii) the topographic highs composed of the Cadiz (CR, Figure 2), Doñana (DR, Figure 2), Guadalquivir (GR, Figure 2) diapiric ridges, and the Guadalquivir Bank (GB, Figure 2); (iii) the smooth areas composed of the Bartolome Dias (BDD, Figure 2), Faro-Cadiz (FCD, Figure 2), Guadalquivir (GD, Figure 2) and Huelva (HD, Figure 2) drifts;

(3) The overflow-sedimentary lobe sector recently interpreted as a Giant Contouritic Levee (Mulder et al., 2003) (CL, Figure 2) partly dissected by the Gil Eanes Channel (GEC, Figure 2) and by secondary channels (SC, Figure 2) and whose western part coincide with the ponded basin area (PB, Figure 2).

The MOW disconnects from the seafloor at around 1200 m and 1500 m water depth in the eastern and western parts of the Gulf, respectively, and becomes a water mass intercalated between the deep and intermediate Atlantic waters (Baringer and Price, 1999; Hernández-Molina et al., 2003). The MOW velocity decreases gradually down to 0.5 m s^{-1} on the middle slope (Kenyon and Belderson, 1973), and 0.2 m s^{-1} off Cape St Vincent (Meincke et al., 1975; Johnson et al., 2002). The progressive MOW velocity decrease leads to particle sorting and induces varied development of sedimentary bodies along its path. In the most proximal part of Gibraltar, the main deposits are coarse-grained sediments with giant furrows, ribbons, and sand waves (Kenyon and Belderson, 1973; Habgood et al., 2003; Mulder et al., 2003) while, downstream, the fine-grained deposits built in silty-clayey contouritic drifts (Gonthier et al., 1984; Faugères et al., 1985a; Stow et al., 1986).

Several studies have been focussed on the sedimentary facies and processes on the Gulf of Cadiz continental slope for about forty years (*e.g.* Heezen and Johnson, 1969; Madelain, 1970; Kenyon and Belderson, 1973; Mélières, 1974; Faugères et al., 1985b; Stow et al., 1986, 2002; Nelson et al., 1993, 1999; Llave et al., 2001, 2006, 2007; Habgood et al., 2003; Hernández-Molina et al., 2003, 2006). Heezen and Johnson (1969) and Kenyon and Belderson (1973) would be the first to identify, from bottom photographs and sidescan sonar images, several provinces characterized by distinct sedimentary features in the middle slope of the Gulf of Cadiz. Save for few modifications introduced to this classification during the nineties, since 2000, more detailed analysis of the slope morphology and the MOW variability, with the identification of new provinces, has become possible using modern acoustic systems (Habgood et al., 2003; Hernández-Molina et al., 2003, 2006; Mulder et al., 2003; Llave et al., 2007 among the more recent studies). Compared to the resolution of these previous acoustic systems (e.g. EM12S-120 multibeam echo-sounder, Seamap and TOBI sidescan sonars), the accuracy of our acoustic data (EM300 and SAR imagery spatial resolution equal to 12.5 m and 0.25 m, respectively) allows, for the first time, a very high resolution characterisation of the seafloor at a regional scale. In this paper, we present a new distribution pattern of the sediments in the eastern part of the Gulf of Cadiz where numerous gravity instabilities are identified, and the close connection between the MOW, the Coriolis force and the seafloor morphology is demonstrated.

2. MATERIAL AND METHODS

The data presented in this paper were collected during the CADISAR Cruise on the RV 'Le Suroît' in August 2001. Bathymetric (Figure 2) and acoustic imagery (Figure 3) data were acquired with a SIMRAD EM300 multibeam echosounder, system operating at a 32 kHz frequency. The spatial and vertical bathymetry resolution is 30 m × 30 m and 2 m, respectively. The imagery spatial resolution is 12.5 m. On the basis of the variations in the backscatter values, interpretation of the acoustic imagery allows to lead to the distribution of the sedimentary facies in the eastern part of the Gulf of Cadiz. EM300 imagery was completed by SAR (*Système Acoustique Remorqué*) imagery (Figure 3), a deep-towed multisensor geophysical tool (Farcy and Voisset, 1985). It is tracked at 100 m above the seafloor and works at a 180 kHz frequency. This system, used to calibrate the multibeam imagery, allows to acquire very high resolution data with a sidescan imagery resolution of 0.25 m and so to accede to the detail morphology of the submarine sedimentary features subjected to the MOW activity. Seismic profiles were acquired from very high resolution sub-bottom profiler operating at a frequency ranging between 2.5 and 3.5 kHz (CHIRP mode). Based on the classification of Damuth and Hayes (1977), which is widely used for classifying deep-ocean sediments using 3.5 kHz echograms, the detailed mapping of the acoustic echofacies in the Gulf of Cadiz from Hanquiez et al. (accepted) is also used. The top of 25 piston cores (Figure 3) were also used to reveal the sediment grain size and to interpret the acoustic imagery.

To quantify the circulation of the MOW in the Gulf of Cadiz, we estimated transport flow velocity parameters. However, the relationship between the particle grain size and current velocities is complex: it depends on the cohesion of the sediments and the possibility for each grain to be transported as a discrete particle, either by bed-load, or in suspension in the nepheloid layer. Current velocities are very fluctuating because of turbulence, the particles are not transported continuously in time (Migeon, 2000). The method we used was proposed by McCave (1984) and consists in evaluating the shearing velocity (U^x in cm s^{-1}) for particles transport. U^x is estimated using the 90th centile (D90) obtained by the granulometric analysis (Table 1). Assumption is made that coarse-grained particles (> 100 µm) are not transported in suspension but only by bed load. U^x is converted into mean transport velocity at 1 m above the seafloor (U in cm s^{-1}, Table 1) from the experimental relationship (Sternberg, 1968):

$U = \sqrt{U^{x2} / C_{100}}$ where C_{100} is the drag coefficient determined at 3.1×10^{-3} by Sternberg.

3. MORPHO-SEDIMENTARY FACIES

3.1. Erosive facies (rocky facies)

The rocky facies is characterized by high “backscatter values” with medium to low backscatter lineaments of about fifty meters wide and 1 to 15 km long similar to the lineaments and the longitudinal furrows observed on the northern Aquitaine shelf (Cirac et al., 1998) and on the Mont-Saint-Michel Bay (Ehrhold et al., 2003) (Table 2). This facies shows a prolonged bottom echo with no reflector below seafloor, and locally some large and irregular overlapping or single hyperbolae with widely varying vertex elevations above the seafloor. This echo shows similarities with echo types IIB and IIIA of Damuth and Hayes (1977). According to the observation of López-Galindo *et al.* (1999), Nelson et al. (1999) and Habgood et al. (2003) in the Gulf of Cadiz, this facies is subdivided into a gravely rock and sandy rock facies, both characterized by longitudinal furrows possibly filled by coarse material.

3.2. Depositional facies

3.2.1. Sand sheets

The sand sheet facies presents a homogeneous low “backscatter values” without apparent structure (Table 2). It is characterized by a continuous, clear bottom echo with no or rare reflectors below seafloor. This facies shows similarities with echo type IA of Damuth and Hayes (1977) and is interpreted as sediment with an important coarse fraction.

3.2.2. Sand ribbons

The sand ribbon facies shows alternation of high and low backscatter stripes (Table 2). The low backscatter features are up to 10 km long and 200 m wide. This facies is characterized by a continuous, clear bottom echo with no reflector below seafloor, like echo type IA of Damuth and Hayes (1977). This facies shows similarities with the banded facies observed and described on continental shelves (e.g., Cirac et al., 1998; Ehrhold et al., 2003; Flemming, 1979). In this area, it corresponds to sand ribbons (Habgood et al., 2003; Mulder et al., 2003) overlying a gravelly substrate which shows up as higher “backscatter values”. The high sand content (89 %) of the CADKS02 core collected in this facies is consistent with this interpretation (Table 1).

3.2.3. Small sand waves

The small sand wave facies shows low “backscatter values” with small straight wavy structures of about 1 to 2 m high and 100 to 200 m wavelength similar with the small dunes described on the northern Aquitaine shelf by Cirac et al. (1998) (Table 2). The CADKS01 core collected in this facies shows a high sand content (87 %) in the surficial sediments (Table 2). This facies shows regular and intense overlapping hyperbolae with vertices approximately tangent to the seafloor. This hyperbolic echoes shows similarities with echo type IIIC of Damuth and Hayes (1977).

3.2.4. Sand waves

The sand wave facies is characterized by low “backscatter values” with wavy structures characterized by amplitude and wavelength ranging from 4 to 10 m and 200 to 300 m, respectively (Table 2). The CADKS03 core acquired in this facies shows coarse surface sediments with sand content of 95 % (Table 1). This facies shows regular slightly overlapping hyperbolae with varying vertex elevation above the seafloor. It shows similarities with echo type IIIC of Damuth and Hayes (1977). The wavy structures are similar to the dunes described on the southeast African continental shelf (Flemming, 1979) and in the entrance to the Gironde Estuary (Berné et al., 1993). In this work, asymmetrical morphology is mainly observed with locally barkhanoïde sand wave fields.

3.2.5. Interfering sand waves

The interfering sand wave facies shows low “backscatter values” with a dense network of straight wavy structures responsible of an embossed morphology (Table 2). Amplitude and wavelength of these bedforms range from 2 to 5 m and 100 to 150 m, respectively. This facies, located in the sandy zones described by Madelain (1970) and Habgood et al. (2003), shows regular overlapping hyperbolae with varying vertex elevation above the seafloor very similar to echo type IIIC of Damuth and Hayes (1977).

3.2.6. Homogeneous mud

The homogeneous mud facies shows a homogeneous medium "backscatter values" without apparent structure (Table 2). It is characterized by a continuous and clear bottom echo with continuous, parallel reflectors below seafloor. It shows similarities with echo type IB of Damuth and Hayes (1977). The top of CADKS22 and CADKS23 cores acquired in this facies shows sediments mainly composed of silt (~50 %) with a clayey fraction higher than 30 % (Table 1).

On the basis of bathymetric data, another facies similar in their acoustic characteristics to the homogeneous mud facies is defined. This facies is characterized by the presence of large kilometric to multi-kilometric depressions and is interpreted as ponded basin deposits (Prather, 2000).

3.2.7. Mud waves

The mud wave facies shows medium "backscatter values" with large undulated wavy structures about 40 m high with a wavelength of 600 m (Table 2). It presents a wavy continuous bottom echo without hyperbolae with continuous, parallel reflectors below seafloor showing similarities with the echo type IB of Damuth and Hayes (1977). These structures correspond to the large mud waves already recognized and described by Kenyon and Belderson (1973), Nelson et al. (1993) and Habgood et al. (2003).

3.3. Instability facies

3.3.1. Sandy instabilities

The sandy instability facies presents heterogeneous "backscatter values" without organized features (Table 2). It shows regular to irregular overlapping hyperbolae with varying vertex elevation above the seafloor. This facies shows similarities with echo type IIIC of Damuth and Hayes (1977) and chaotic facies described by Cochonat and Ollier (1987).

3.3.2. Muddy instabilities

The muddy instability facies shows low to medium “backscatter values” with numerous multi-hectometric curvilinear structures characterized by low to high “backscatter values” (Table 2). It shows regular to irregular overlapping hyperbolae with varying vertex elevation above the seafloor, like echo type IIIC of Damuth and Hayes (1977). Due to the similarities with the sandy instabilities and the observation previously made by Mulder et al. (2003), this facies is interpreted as failure scars and mass flow deposits. On the basis of backscatter variation and lithologic interpretation of Habgood et al. (2003), two subdivision are defined: (1) the muddy sand instabilities, characterized by low “backscatter values” and a medium to high sand content, and (2) the muddy instabilities, characterized by medium “backscatter values” with a low sand content and a low number of curvilinear structures.

4. DISTRIBUTION OF THE SEDIMENTARY PROCESSES

4.1. Proximal scour and sand-ribbons sector

The south-eastern part of the Main MOW Channel presents erosive furrows related to intense current activity (Kenyon and Belderson, 1973; Belderson et al., 1982; Turcq, 1984). This sector, also characterized by rock outcrops and gravel, shows evidence of an erosive action of the MOW on the seafloor (Figure 4).

North of the NNE/SSW concave trench (Figure 2), the MMC is entirely covered by the sandy facies. The type of sandy facies evolves both northward and westward. On section beginning in the gravel sector and ending with the Cadiz Channel and the Giant Contouritic Levee, the observed erosional/depositional bedforms are due to the activity of bottom currents (Heezen et al., 1966; Hollister et al., 1974). We find successively sand ribbons, small sand waves and straight or interfering sand waves (Figures 4 and 5). The sand ribbons and the few furrows, observed close to the rock outcrop and gravel area, indicate a transition zone where both erosion and deposition occur. Orientation of these bedforms (110°N and 140°N, south and north of 36°N, respectively) shows a progressive northwestward bending in a clockwise direction of the MOW ending around 36°02'N/6°48'W (Figure 4). At this location, disappearance of the furrows coincides with the edification of sand waves. These sand waves show crests orientated 35°N to 45°N in the central sector of the Main MOW Channel, and 5°N close to the Giant Contouritic Levee. This change in crest orientation shows a progressive westward bending in an anticlockwise direction of the MOW. These sand waves can morphologically be associated with the washed-out dunes of Simons and Richardson (1961) and illustrate the predominance of depositional processes and the decrease of the MOW velocity. The bedform morphology indicates a current flowing towards 310°N. Westward, the higher amplitude of the sand waves indicates a decrease of the MOW velocity, according to the bedform classification of Simons and Richardson (1961).

The interfering sand waves observed in the northern part of the Main MOW Channel indicates bi-directional currents at this location. Orientation of a part of the wave crests (towards 65°N) is consistent with a northwestward direction for the MOW. The orientation of the remaining wave crests (towards 25°N) show a westward MOW component and indicates that the SMB have already an effect on the seafloor before to be channelized by the Cadiz Channel.

4.2. Channels and ridges sector

The Cadiz Contourite Channel is characterized by rock outcrops and sandy sediments sometimes with sedimentary structures (Figures 4, 6 and 7). Rock outcrops are mainly located along the Cadiz and Guadalquivir ridges, so locally showing the sediment stratification (Figure 6B). East of 7°30’W, the channel is dissected by furrows orientated 285°N west of the Cadiz Ridge, and 40°N to 60°N along the Guadalquivir Ridge. From 10°N to 20°N in the upstream part of the channel and 150°N along the Guadalquivir Ridge, the wave crest orientation is about 5°N just west of 7°35’W. Change in orientation of these structures shows the southwestward bending in an anticlockwise direction of the SMB along the upstream part of the Cadiz Contourite Channel, then the northwestward bending in a clockwise direction of the SMB along the downstream part of this channel (Figure 4). A westward decrease of the sand wave amplitude is also observed along the channel pathway. This decrease continues until the complete disappearance of these bedforms at 7°47’W (Figure 7C). These sand waves are mainly straight crests with the exception of a small barchan field focussed around 36°12’N/7°45’W (Figure 7A). The westward reduction of the bedform amplitude, the lack of dynamic structures in the downstream part of the Cadiz Channel, and the fine-grained sediments observed from 7°55’W (Figure 4) indicate a westward decrease of the SMB competence and velocity.

The Huelva Contourite Channel has a similar sedimentary facies evolution west of the Cadiz and Guadalquivir diapiric ridge rock outcrops. At the western limit of the ridges, the channel floor exhibits sand facies without bedform, and then homogeneous mud, so displaying the nothwestward decrease of the IMB velocity (Figure 4). Rare furrows orientated 120°N observed along the channel course testify of an erosive action of the IMB (Figure 4).

The Guadalquivir Contourite Channel is mainly characterized by sand deposits in its upstream part (Figure 4). This facies is present in two secondary branches surrounding a muddy area with smooth morphology between 7°25’W and 7°40’W (Mulder et al., 2003) (Figure 4). In the northern branch, thin furrows orientated 60°N to 80°N are observed (Figure 8). From 7°35’W, convergence of these two branches is associated with apparition of rock outcrops along the channel course, so showing an acceleration of the PMB at this location (Figure 4). The 120°N orientated furrows observed in the distal part of the Guadalquivir Contourite Channel corroborate this interpretation (Figure 4).

Between the main contourite channels, contourite drifts are mainly characterized by fine-grained deposits without dynamic structures, evidence of dominance of deposit processes and low MOW activity in these areas (Figure 4). Only the south-eastern part of the Huelva drift and the southern part of the Guadalquivir drift have sandy surficial deposits. Muddy instabilities can be observed on the southeastern edge of the Bartolome Dias Drift, just east of the Guadalquivir Bank (Figure 4). These semicircle scars, joined and parallel to the right flank of the Guadalquivir Channel, appear related to gravity mass flows (Embley and Hayes, 1976; Jacobi, 1976; Damuth, 1980).

4.3. Overflow-sedimentary lobe sector

This sector, previously described as a mud wave to muddy sand wave area (Kenyon and Belderson, 1973; Nelson et al., 1993, 1999; Habgood et al., 2003) contains numerous instabilities in addition to sedimentary structures (Mulder et al., 2003; Hernández-Molina et al., 2003) (Figure 4). In detail, muddy sand instabilities are mainly observed: (1) along the southern edge of the Cadiz Channel and the western edge of the Main MOW Channel (Figure 9A), (2) on the right levee of the Gil Eanes Channel (Figure 10), (3) along and at the mouth of the secondary channels disconnected to the Main MOW Channel, north of the Gil Eanes Channel (Figure 9B), and (4) on both sides of the secondary channels connected to the Main MOW Channel, south of the Gil Eanes Channel (Figure 9C and Figure 11A-B). Muddy instabilities cover the rest of the Giant Contouritic Levee, except in areas around 35°52’N/7°W and 35°52’N/7°24’W, which are covered by mud waves with 15°N to 30°N orientated crests (Figure 4). All these instabilities reflect the dominance of gravity processes on the Giant Contouritic Levee.

Orientation and continuity of the sand waves, observed in the western part of the Main MOW Channel, at the end of the southern secondary channels (Figure 11A-B), and along the Gil Eanes Channel (Figure 10), indicate action of the MOW in these channels and the westward bending in an anticlockwise direction of this current over the Giant contouritic Levee. Locally, sand waves are also observed on the edges of the secondary channels and have crests sub-parallel to the channel axis (Figure 9C and Figure 11B). In the Gil Eanes Channel, sand waves are associated with narrow sand-filled furrows (25 m width) and scours, which are concentrated along the outer part of the meanders (Figure 10). From 7°12’W, the Gil Eanes Channel is floored by sand deposits without bedforms, suggesting a south-westward decrease in flow intensity. The sand sheet developed at its mouth is interpreted as gravity depositional lobes (Habgood et al., 2003) (Figure 4).

5. Discussion

5.1. Hydrodynamics of the MOW

If it is usual that the sedimentary features commonly associated with bottom currents (e.g. mud waves) are generally oblique to flow direction, in our study, the bedform crests are almost perpendicular to the MOW direction. This statement is confirmed in the channelized areas (Main MOW Channel, Cadiz, Huelva and Guadalquivir contourite channels) where the MOW acts as an unidirectional current. Opposite, in the spilling zones like the Giant Contouritic Levee (Mulder et al., 2003), the strong change between the channel and levee slopes and the multidirectional nature of the MOW could explain the oblique direction of the large bedform crests compared to the general MOW flow.

Using the relationship of Sternberg (1968) to estimate the MOW transport velocity values and the orientation of furrows and wave crests displayed in the study area, a semi quantitative model of the MOW velocity evolution is established in the eastern part of the Gulf of Cadiz and shows the northward and westward decrease of the MOW energy (Figure 12). Highest velocities, ranging from 115 to 200 cm s^{-1}, are in the south-eastern part of the Main MOW Channel. They are consistent with the velocities previously measured by Heezen and Johnson (1969), Madelain (1970) and Baringer and Price (1999) and are also in agreement with the velocity threshold to generate erosive furrows and sand ribbons (Dyer, 1970; Belderson et al., 1982). Downstream, around the Main MOW and Cadiz channel junction, velocities range from 25 to 70 cm s^{-1} and are of the same order that the values of Ambar and Howe (1979) and Baringer and Price (1999). After our estimations, the central part of the Guadalquivir Channel should be characterized by velocities ranging from 18 to 36 cm s^{-1}, and about 14 cm s^{-1} on the outer flank of the Giant Contouritic Levee.

5.2. Impact of the seafloor and the Coriolis force on the MOW pathway

Erosion of the SMB and PMB observed along the Cadiz and Guadalquivir channels is related to a reduction of the MOW section near the Cadiz and Guadalquivir ridges and Guadalquivir Bank, around 36°14’N/7°02’W (c1, Figure 2), 36°17’N/7°20’W (c2, Figure 2) and 36°24’N/7°38’W (c3, Figure 2), which induces an increase of the SMB and PMB velocities. In addition, the erosive action of these two branches is emphasized by the Coriolis force which plasters the MOW against these ridges. Change in furrow orientation observed along the Cadiz and Guadalquivir channels shows that the SMB and PMB follows the pathway defined by these tectonic highs, thus confirming the previous observations of Nelson et al. (1999) (Figure 12).

The muddy nature of the Faro-Cadiz Drift shows that the IMB stays confined in the Huelva Channel along its path. The presence of fine-grained deposits between 7°08’W and 7°10’W and sandy sediments west of the Guadalquivir Ridge suggests a decrease and then an increase of the IMB competence because of the reduction of the flowing section at 36°25’N/7°10’W (c4, Figure 2). The sandy nature of the southern part of the Faro-Cadiz Drift shows that a part of the IMB circulates westward, due to the proximity of the Guadalquivir ridge. Passed the Guadalquivir Ridge, the IMB remains confined into the Guadalquivir Channel where it forms the PMB. This suggests that the divergence between the IMB and the PMB takes place around 36°21’N/7°07’W. Downstream, in the central part of the Guadalquivir Channel, the development of a second sandy area west of the Doñana Ridge shows that this tectonic structure is responsible of the PMB dichotomy.

The sandy nature of the north flank of the Guadalquivir Ridge indicates that a part of the SMB spills over this tectonic high around 7°30’W. Consequently, the Guadalquivir Drift is partly built by the SMB. This spilling is related both to the inertia of the overall westward oriented SMB between 7°05’W and 7°20’W and to the Coriolis force which orientates the SMB circulation towards the north. In addition, action of the Coriolis force is visible from 7°35’W by the northwestward bending in a clockwise direction of the MOW on reaching the western limit of the Guadalquivir Ridge. This MOW bending is also consistent with the end of the confinement of the SMB in the Cadiz Channel.

5.3. Interaction between gravity and contouritic processes

The presence of rock outcrops and sandy material along the submarine valleys bordering the western flank of the Cadiz and Guadalquivir ridges (Figure 12) indicates an erosive action of the currents channelized in these valleys. These valleys, described as marginal valleys by García (2002) and Hernández-Molina et al. (2003), seem to connect the different MLW branches and to transit sediments from the shelf to the slope in the form of gravity currents.

The numerous failure scars observed on the right levee of the Gil Eanes Channel are related to high sedimentation rate due to the spilling of the channelized MOW (Mulder et al., 2003). This is confirmed downstream by both the splayed shape of the large mud wave field and the mud wave crest orientation that is sub-perpendicular to the channel axis. This associated to the presence of distal sandy lobes suggest many similarities between the Gil Eanes Channel and channels found in deep-sea turbidite systems (Normark, 1978; Walker, 1978; Normark et al., 1993). However, due to the permanent circulation of the MOW, the Gil Eanes Channel is interpreted as a typical channel draining downwelling currents (Faugères et al., 1999; Habgood et al., 2003; Mulder et al., 2003). The presence of the previous mud wave field can also be related to the combined action of the MOW which spills over the Giant Contouritic Levee and is responsible for the numerous failure scars observed in this area (Mulder et al., 2003). This is strengthened by the presence of large mud waves south of the connected secondary channels. Reduction of failure scar number and change from muddy sand to muddy deposits in the central and western parts of the Giant Contouritic Levee suggest the westward decrease of the shearing, velocity and competence of the MOW. Sandy instabilities, presented west of the Main MOW Channel, and muddy instabilities, observed on the southeastern edge of the Bartolome Dias Drift, also testify of the interaction between the MOW and gravity processes.

6. CONCLUSION

The new high resolution sedimentary facies distribution proposed in this study completes, details, and corrects the previous models established in the eastern part of the Gulf of Cadiz and allows a better understanding of the processes acting in this system. High quality of the imagery data (EM300 and SAR imagery spatial resolution equal to 12.5 m and 0.25 m, respectively) allows a precise characterization of the diverse bedforms built by the MOW along its path, and an accurate definition of their spatial limits. Sandy deposits are confined in the whole contouritic channels, the Gil Eanes channel and the secondary channels connected to the Main MOW Channel. Bedform changes, deposit lithology, and estimated MOW transport velocities confirm the northward and westward decrease of the MOW energy and competence. Although most of the previous works reveal the sandy nature of the main MOW channel, our study shows, for the first time, the progressive northward and westward evolution of the bedforms along the Main MOW Channel with erosive furrows, sand ribbons, small sand waves, and symmetrical to interfering sand waves. Our study emphasizes the major role of the seafloor morphology, especially the tectonic highs, which determines the MOW pathway and varies the current intensity. The still erosive action of the MOW south of the Guadalquivir Bank, and the evolution of the deposits along the Cadiz Channel (sand waves, sand sheets, and homogeneous mud) are shown. Moreover, the mud wave and muddy sand wave area described in the previous works corresponds, in reality, to an unstable muddy sand sector where gravity processes and MOW flow interact. Finally, estimation method of the current MOW velocities could be enlarged to the past sedimentation in order to improve the paleoenvironmental reconstructions in an area important for the study of the Atlantic/Mediterranean exchanges.

ACKNOWLEDGMENTS

The authors thank GENAVIR and the crew of the RV "Le Suroît" for technical assistance during the CADISAR cruise. We gratefully thank anonymous reviewer, M. Rebesco, and the editor for their helpful comments to this manuscript. This is an UMR/CNRS EPOC 5805 contribution n° 1620.

REFERENCES

Ambar, I., Armi, L., Bower, A. and Ferreira, T., 1999. Some aspects of time variability of the Mediterranean Water off south Portugal. Deep Sea Research Part I: Oceanographic Research Papers, 46, 1109-1136.

Ambar, I. and Howe, M.R., 1979. Observations of the Mediterranean outflow. II. The deep circulation in the vicinity of the Gulf of Cadiz. Deep Sea Research Part A. Oceanographic Research Papers, 26, 555-568.

Baringer, M.O., 1993. Mixing and Dynamics of the Mediterranean Outflow, PhD Thesis, Mass. Inst. of Technol./Woods Hole Oceanogr. Inst. Joint Program, Cambridge, Mass., WHOI-93-52, 244 pp.

Baringer, M.O. and Price, J.F., 1999. A review of the physical oceanography of the Mediterranean outflow. Marine Geology, 155, 63-82.

Belderson, R.H., Johnson, M.A. and Kenyon, N., 1982. Bedforms. In: A.H. Stride (Ed), Offshore Tidal Sands: Processes and Deposits. Chapman and Hall, London, pp. 27-57.

Berné, S., Castaing, P., Le Drezen, E. and Lericolais, G., 1993. Morphology, internal structure, and reversal of asymmetry of large subtidal dunes in the entrance to Gironde Estuary (France). Journal of sedimentary Petrology, 63, 780-793.

Borenäs, K.M., Wahlin, A.K., Ambar, I. and Serra, N., 2002. The Mediterranean outflow splitting--a comparison between theoretical models and CANIGO data. Deep Sea Research Part II: Topical Studies in Oceanography, 49, 4195-4205.

Bower, A.S., Armi, L. and Ambar, I., 1997. Lagrangian observations of meddy formation during a Mediterranean undercurrent seeding experiment. Journal of Physical Oceanography, 27, 2545-2575.

Boyum, G., 1967. Hydrological observations of the M/S Helland-Hansen and current measurements in the area west of Gibraltar, May 1965. NATO Sub-Comm. Oceanogr. Research Technical Report, 34, 35-36.

Cirac, P., Berné, S., Castaing, P. and Weber, O., 1998. Processus de mise en place et d'évolution de la couverture sédimentaire superficielle de la plate-forme nord-aquitaine. Oceanologica Acta, 23, 663-686.

Cochonat, P. and Ollier, G., 1987. Interprétation géologique des images SAR. Données de l'opération TITANIC, rapport scientifique et technique de l'Ifremer, 4, 66 pp.

Damuth, J.E., 1980. Use of high-frequency (3.5-12 kHz) echograms in the study of near-bottom sedimentation processes in the deep-sea: A review. Marine Geology, 38, 51-75.

Damuth, J.E. and Hayes, D.E., 1977. Echo character of the East Brazilian continental margin and its relationship to sedimentary processes. Marine Geology, 24, 73-95.

Dyer, K.E., 1970. Linear erosional furrows in Southampton water. Nature, 225, 56-58.

Ehrhold, A., Guillou, S., Auffret, J.P., Garlan, T. and Dan Nguyen, K., 2003. Bedload transport modelisation in a bay characterized by a macrotidal environment: example of the Mont-Saint-Michel Bay (Manche, France). Oceanologica Acta, 26, 443-455.

Embley, R.W. and Hayes, D.E., 1976. New evidence for occurrence of debris flow deposits in the deep sea. Geology, 4, 371-374.

Farcy, A. and Voisset, M., 1985. Acoustic imagery of sea floor. In: V.C. Anderson (Ed), Oceans `85: Ocean Engineering and the Environment, New York (IEEE), pp. 1005-1012.

Faugères, J.-C., Cremer, M., Monteiro, J.H. and Gaspar, L., 1985a. Essai de reconstitution des processus d'édification de la ride sédimentaire de Faro (marge sud-portugaise). Bulletin de l'Institut de Géologie du Bassin d'Aquitaine, 37, 229-258.

Faugères, J.-C., Frappa, M., Gonthier, E. and Grousset, F.E., 1985b. Impact de la veine d'eau méditerranéenne sur la sédimentation de la marge sud et ouest ibérique au quaternaire récent. Bulletin de l'Institut de Géologie du Bassin d'Aquitaine, 37, 259-287.

Faugères, J.-C., Stow, D.A.V., Imbert, P. and Viana, A., 1999. Seismic features diagnostic of contourite drifts. Marine Geology, 162, 1-38.

Flemming, B.W., 1979. Sand transport and bedform patterns on the continental shelf between Durban and Port Elizabeth (southeast African continental margin). Sedimentary Geology, 26, 179-205.

García, M., 2002. Caracterización morfológica del sistema de canales y valles submarinos del talud medio del Golfo de Cádiz (SO de la Península Iberica): implicaciones oceanográficas, Tesis de Licenciatura, Facultad de Ciencas del Mar, Univ. Cádiz, 114 pp.

Gardner, J.V. and Kidd, R.B., 1983. Sedimentary processes on the Iberian continental margin viewed by long-range side-scan sonar. 1: Gulf of Cadiz. Oceanologica Acta, 6, 245-254.

Gonthier, E., Faugères, J.-C. and Stow, D.A.V., 1984. Contourite facies of the Faro drift, Gulf of Cadiz. In: D.A.V. Stow and D.J.W. Piper (Eds), Fine-Grained

Sediments : Deep Water Processes and Facies. Geologica Society by Blackwell Scientific Publications, Oxford London Edinburg, pp. 245 -256.

Habgood, E.L., Kenyon, N.H., Masson, D.G., Akhmetzhanov, A., Weaver, P.P.E., Gardner, J.M. and Mulder, T., 2003. Deep-water sediment wave fields, bottom current sand channels and gravity flow channel-lobe systems: Gulf of Cadiz, NE Atlantic. Sedimentology, 50, 483-510.

Hanquiez, V., Mulder, T., Lecroart, P., Voisset, M., Gonthier, E., Marches, E. and Girardi, A. Chirp echo characters of the surficial sediments in the eastern Gulf of Cadiz (NE Atlantic). Geo-Marine Letters, accepted.

Heezen, B.C., Hollister, C.D. and Ruddiman, W.F., 1966. Shaping of the continental rise by deep geostrophic contour currents. Science, 152, 502-508.

Heezen, B.C. and Johnson, G.L., 1969. Mediterranean under-current and microphysiography west of Gibraltar. Bulletins de l'Institut Oceanographique de Monaco, 67, 1-97.

Hernández-Molina, F.J., Llave, E., Somoza, L., Fernandez-Puga, M.C., Maestro, A., León, R., Medialdea, T., Barnolas, A., Garcia, M., Díaz-del-Río, V., Fernandez-Salas, L.M., Vázquez, J.T., Lobo, F.J., Alveirinho Dias, J.M., Rodero, J. and Gardner, J.M., 2003. Loocking for clues to paleoceanographic imprits: A diagnosis of the Gulf of Cadiz contourite depositional systems. Geology, 31, 19-22.

Hernández-Molina, F.J., Llave, E., Stow, D.A.V., Garcia, M., Somoza, L., Vazquez, J.T., Lobo, F.J., Maestro, A., Diaz del Rio, V. and Leon, R., 2006. The contourite depositional system of the Gulf of Cadiz: A sedimentary model related to the bottom current activity of the Mediterranean outflow water and its interaction with the continental margin. Deep Sea Research Part II: Topical Studies in Oceanography, 53, 1420-1463.

Hollister, C.D., Flood, R.D., Johnson, D.A., Lonsdale, P. and Southard, J.B., 1974. Abyssal furrows and hyperbolic echo traces on the Bahama Outer Ridge. Geology, 2, 395-400.

Jacobi, R.D., 1976. Sediment slides on the northwestern continental margin of Africa. Marine Geology, 22, 157-173.

Johnson, J., Ambar, I., Serra, N. and Stevens, I., 2002. Comparative studies of the spreading of Mediterranean water through the Gulf of Cadiz. Deep Sea Research Part II: Topical Studies in Oceanography, 49, 4179-4193.

Johnson, J. and Stevens, I., 2000. A fine resolution model of the eastern North Atlantic between the Azores, the Canary Islands and the Gibraltar Strait. Deep-Sea Research Part I: Oceanographic Research Papers, 47, 875-899.

Kenyon, N.H. and Belderson, R.H., 1973. Bed forms of the Mediterranean undercurrent observed with side-scan sonar. Sedimentary Geology, 9, 77-99.

Llave, E., Hernández-Molina, F.J., Somoza, L., Díaz-del-Río, V., Stow, D.A.V., Maestro, A. and Dias, J.M.A., 2001. Seismic stacking pattern of the Faro-Albufeira contourite system (Gulf of Cadiz): a Quaternary record of paleoceanographic and tectonic influences. Marine Geophysical Researches, 22, 487-508.

Llave, E., Hernández-Molina, F.J., Somoza, L., Stow, D.A.V. and Diaz del Rio, V., 2007. Quaternary evolution of the Contourite Depositional System in the Gulf of Cadiz. In: A. Viana and M. Rebesco (Eds), Economic and Paleoceanographic Importance of Contourites. Geological Society of London, Special Publication, pp. 49-80.

Llave, E., Schönfeld, J., Hernandez-Molina, F.J., Mulder, T., Somoza, L., Diaz del Rio, V. and Sanchez-Almazo, I., 2006. High-resolution stratigraphy of the Mediterranean outflow contourite system in the Gulf of Cadiz during the late Pleistocene: The impact of Heinrich events. Marine Geology, 227, 241-262.

Lopez-Galindo, A., Rodero, J. and Maldonado, A., 1999. Surface facies and sediment dispersal patterns: southeastern Gulf of Cadiz, Spanish continental margin. Marine Geology, 155, 83-98.

Madelain, F., 1970. Influence de la topographie du fond sur l'écoulement méditerranéen entre le détroit de Gibraltar et le cap Saint-Vincent. Cahiers Océanographiques, 22, 43-61.

Maldonado, A. and Nelson, C.H., 1999. Interaction of tectonic and depositional processes that control the evolution of the Iberian Gulf of Cadiz margin. Marine Geology, 155, 217-242.

McCave, I.N., 1984. Erosion, transport and deposition of fine-grained marine sediments. In: D.A.V. Stow and D.J.W. Piper (Eds), Fine-Grained Sediments: Deep Water Processes and Facies. The Geological Society of London, Special Publication, pp. 35-69.

Meincke, J., Siedler, G. and Zenk, W., 1975. Some current observations near the continental slope off Portugal. "Meteor"Forsch.-Ergebnisse, 16, 15-22.

Mélières, F., 1974. Recherches sur la dynamique sédimentaire du Golfe de Cadix (Espagne), Thèse d'Etat de l'Université Pierre et Marie Curie, Paris, 235 pp.

Migeon, S., 2000. Dunes géantes et levées sédimentaires en domaine marin profond: approche morphologique, sismique et sédimentologique, Thèse de 3ème cycle, Université Bordeaux 1, Talence.

Mulder, T., Voisset, M., Lecroart, P., Le Drezen, E., Gonthier, E., Hanquiez, V., Faugères, J.-C., Habgood, E.L., Hernández-Molina, F.J., Estrada, F., Llave-Barranco, E., Poirier, D., Gorini, C., Fuchey, Y., Voelker, A., Freitas, P., Lobo Sanchez, F.J., Fernandez, L.M., Kenyon, N.H. and Morel, J., 2003. The Gulf of Cadiz: an unstable giant contouritc levee. Geo-Marine Letters, 23, 7-18.

Nelson, C.H., Baraza, J. and Maldonado, A., 1993. Mediterranean undercurrent sandy contourites, Gulf of Cadiz, Spain. Sedimentary Geology, 82, 103 -131.

Nelson, C.H., Baraza, J., Maldonado, A., Rodero, J., Escutia, C. and Barber, J.H., 1999. Influence of the Atlantic inflow and Mediterranean outflow currents on Late Quaternary sedimentary facies of the Gulf of Cadiz continental margin. Marine Geology, 155, 99-129.

Normark, W.R., 1978. Fan valleys, channels, and depositional lobes on modern submarine fans : Characters for recognition of sandy turbidite environments. Bulletin of the American Association of Petroleum Geologists, 62, 912-931.

Normark, W.R., Posamentier, H. and Mutti, E., 1993. Turbidite systems: State of the art and future directions. Reviews of Geophysics, 31, 91-116.

Ochoa, J. and Bray, N.A., 1991. Water mass exchange in the Gulf of Cadiz. Deep Sea Research, 38, 5465-5503.

Prather, B.E., 2000. Calibration and visualization of depositional process models for above-grade slopes: a case study from the Gulf of Mexico. Marine and Petroleum Geology, 17, 619-638.

Sartori, R., Torelli, L., Zitellini, N., Peis, D. and Lodolo, E., 1994. Eastern segment of the Azores-Gibraltar line (central-eastern Atlantic): An oceanic plate boundary with diffuse compressional deformation. Geology, 22, 555-558.

Simons, D.B. and Richardson, E.V., 1961. Forms of bed roughness in alluvial channels. Journal of the Hydraulics Div., ASCE, 87(HY3), 87-105.

Srivastava, S.P., Shouten, H., Roest, W.R., Klitgord, K.D., Kovacs, L.C., Verhoef, J. and Macnab, R., 1990. Iberian plate kinematics: a jumping plate boundary between Eurasia and Africa. Nature, 344, 756-759.

Sternberg, R.W., 1968. Frictions factors in tidal channels with differing bed roughness. Marine Geology, 6, 242-260.

Stow, D.A.V., Faugères, J.-C. and Gonthier, E., 1986. Facies distribution and textural variation in Faro Drift contourites : velocity fluctuation and drift growth. Marine Geology, 72, 71-100.

Stow, D.A.V., Faugères, J.-C., Gonthier, E., Cremer, M., Llave, E., Hernández-Molina, F.J., Somoza, L. and Díaz-del-Río, V., 2002. Faro-Albufeira drift complex, northern Gulf of Cadiz. In: D.A.V. Stow, C.J. Pudsey, J.A. Howe, J.-C. Faugères and A.R. Viana (Eds), Deep-water contourite systems: modern drifts and ancient series, seismic and sedimentary characteristics. Geological Society of London, London, UK, pp. 137-154.

Turcq, B., 1984. Les faciès sédimentaires du plateau continental nord-aquitain : réponse aux processus hydrodynamiques actuels, Thèse de 3ème cycle, Université Bordeaux 1.

Walker, R.G., 1978. Deep-water sandstone facies and ancient submarine fans: model for exploration for stratigraphic traps. Bulletin of the American Association of Petroleum Geologists, 62, 932-966.

Zenk, W., 1975. On the Mediterranean outflow west of Gibraltar. "Meteor"Forsch.-Ergebnisse, 16, 23-34.

Zenk, W. and Armi, L., 1990. The complex spreading patterns of Mediterranean water off the Portuguese continental slope. Deep Sea Research, 37, 1805-1823.

FIGURE LEGENDS

Figure 1. Map of the Gulf of Cadiz showing the general MOW pathway (grey area); black dotted arrows indicate MOW direction; black arrows indicate Atlantic Inflow direction; IMB: Intermediate MOW Branch; MLW: Mediterranean Lower Water; MUW: Mediterranean Upper Water; MMB: Main MOW Branch; PMB: Principal

MOW Branch; SMB: Southern MOW Branch. Modified from Madelain (1970) and Hernández-Molina et al. (2003).

Figure 2. High resolution EM300 illuminated color-shaded map of the studied area during the CADISAR cruise. BDD: Bartolome Dias Drift; CC: Cadiz Contourite Channel; CL: Giant Contouritic Levee; CR: Cadiz Ridge; c1 to c4: constriction points; DR: Doñana Ridge; FCD: Faro-Cadiz Drift; GB: Guadalquivir Bank; GC: Guadalquivir Contourite Channel; GD: Guadalquivir Drift; GEC: Gil Eanes Channel; GR: Guadalquivir Ridge; HC: Huelva Channel; HD: Huelva Drift; MMC: Main MOW Channel; PB: ponded basins; SC: secondary channels; t: trench. Numbers 1, 2 and 3 are morpho-sedimentary sectors defined by Hernández-Molina et al. (2003); 1: proximal scour and sand-ribbons sector; 2: channels and ridges sector; 3: overflow-sedimentary lobe sector.

Figure 3. High resolution EM300 and SAR acoustic imagery map of the area studied during the CADISAR cruise. Red numbers are core location. Boxes are SAR image location.

Figure 4. Sedimentary facies distribution in the eastern part of the Gulf of Cadiz based on the acoustic imagery interpretation.

Figure 5. SAR images and interpretations showing erosive and deposit bedforms on the Main MOW Channel (see location in Figure 3). White arrows are current directions.

Figure 6. SAR images and interpretations illustrating the bend and the erosive nature of the SMB in the Cadiz Channel (see location in Figure 3). White arrows are current directions.

Figure 7. SAR images and interpretations displaying the lateral facies variation across the downstream part of the Cadiz Channel and the progressive northwestward bend of the SMB (see location in Figure 3). White arrows are current directions.

Figure 8. SAR image and interpretation showing the slightly erosive nature of the PMB along the central part of the Guadalquivir Channel (see location in Figure 3). White arrow is current direction.

Figure 9. SAR images and interpretations showing instabilities on the Giant Contouritic Levee on the western bank of the Main MOW Channel (see location in Figure 3). White arrows are current directions.

Figure 10. SAR image and interpretation illustrating the bedform variability across the Gil Eanes Channel (see location in Figure 3). White arrow is current direction.

Figure 11. SAR imageries and interpretations of the bedforms identified along the secondary channels connected to the Main MOW Channel (see location in Figure 3). White arrows are current directions.

Figure 12. Semi quantitative hydrodynamic model in the eastern part of the Gulf of Cadiz. Black, white and red arrows are MOW directions. Yellow arrows are gravity current directions. Black and white arrows respectively represent minimal and maximal transport velocities (*U*). Vector direction is deduced from bedform orientations.

TABLES

Table 1. Major grain-size classes of surficial sediments and Shearing (*U**) and transport (*U*) velocities calculated from the Sternberg (1968) and McCave (1984) methods (core location in Figure 3).

Table 2. Sedimentary facies classification based on EM300, SAR, chirp and core data.

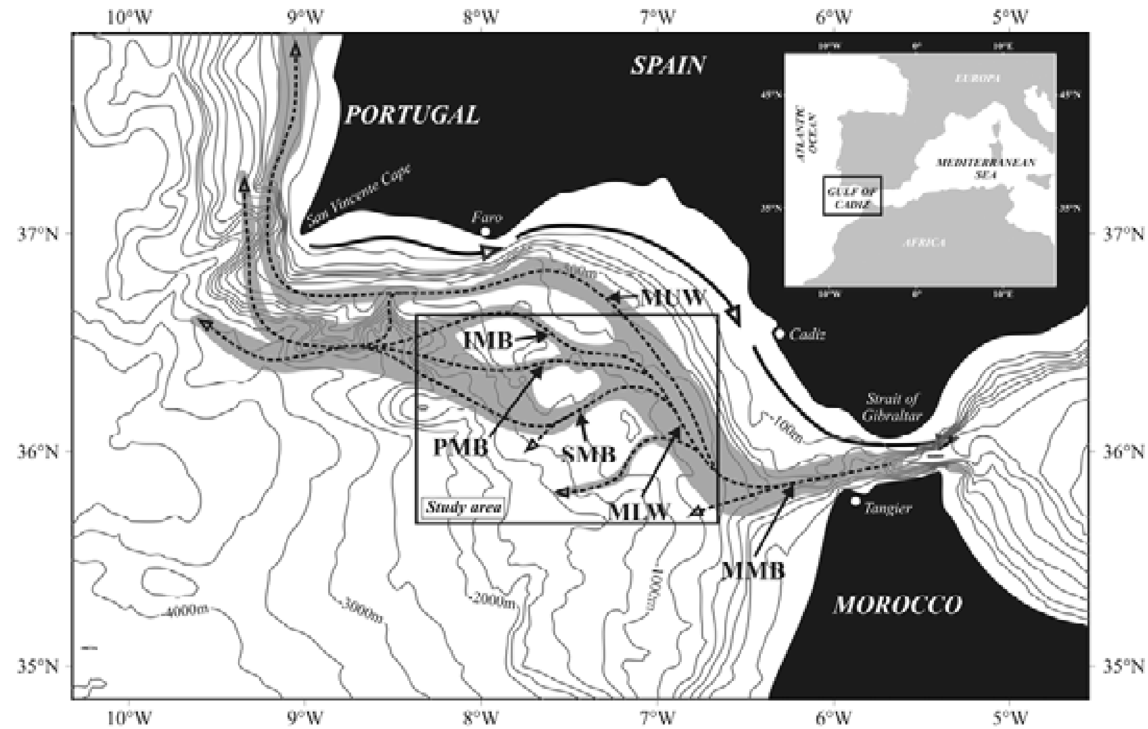
10°W
9°W
8°W
7°W
6°W
5°W
37°N
36°N
35°N
SPAIN
PORTUGAL
San Vincente Cape
Faro
MUW
Cadiz
IMB
PMB
SMB
MLW
MMB
Study area
Strait of Gibraltar
Tangier
MOROCCO
100m
4000m
3000m
2000m
1000m
ATLANTIC OCEAN
EUROPA
MEDITERRANEAN SEA
GULF OF CADIZ
AFRICA

Figure 1

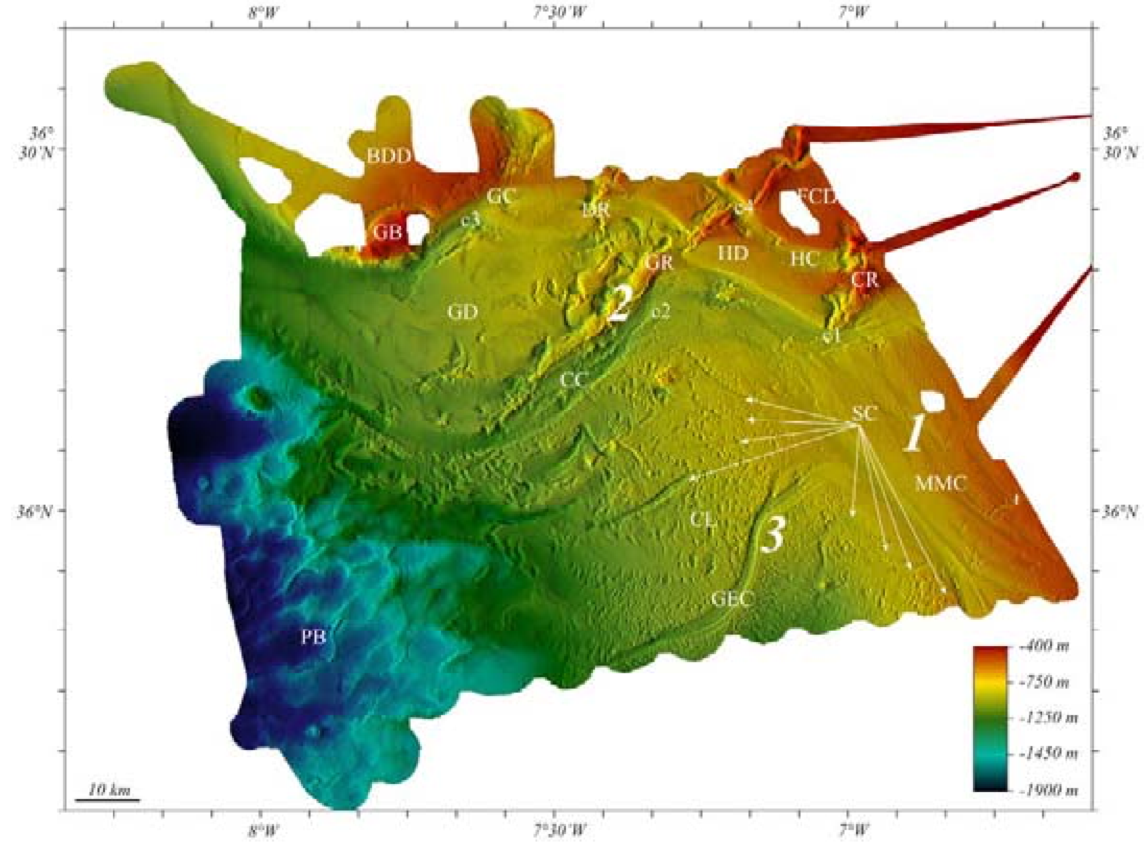
8°W
7°30'W
7°W
36° 30'N
36°N
BDD
GB
GC
c3
DR
GR
2
c2
c4
FCD
HD
HC
CR
c1
GD
CC
SC
1
MMC
CL
3
GEC
PB
-400 m
-750 m
-1250 m
-1450 m
-1900 m
10 km

Figure 2

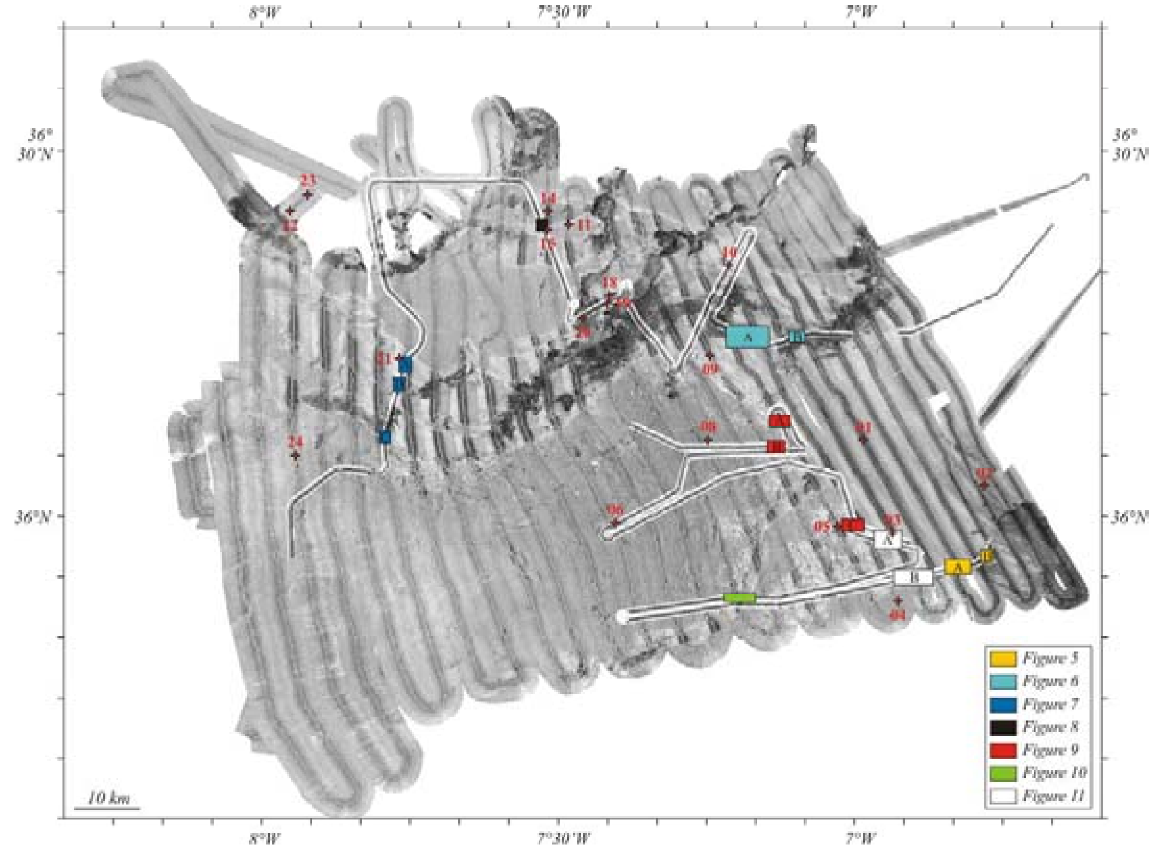
8°W
7°30'W
7°W
36° 30'N
36°N
10 km
Figure 5
Figure 6
Figure 7
Figure 8
Figure 9
Figure 10
Figure 11

Figure 3

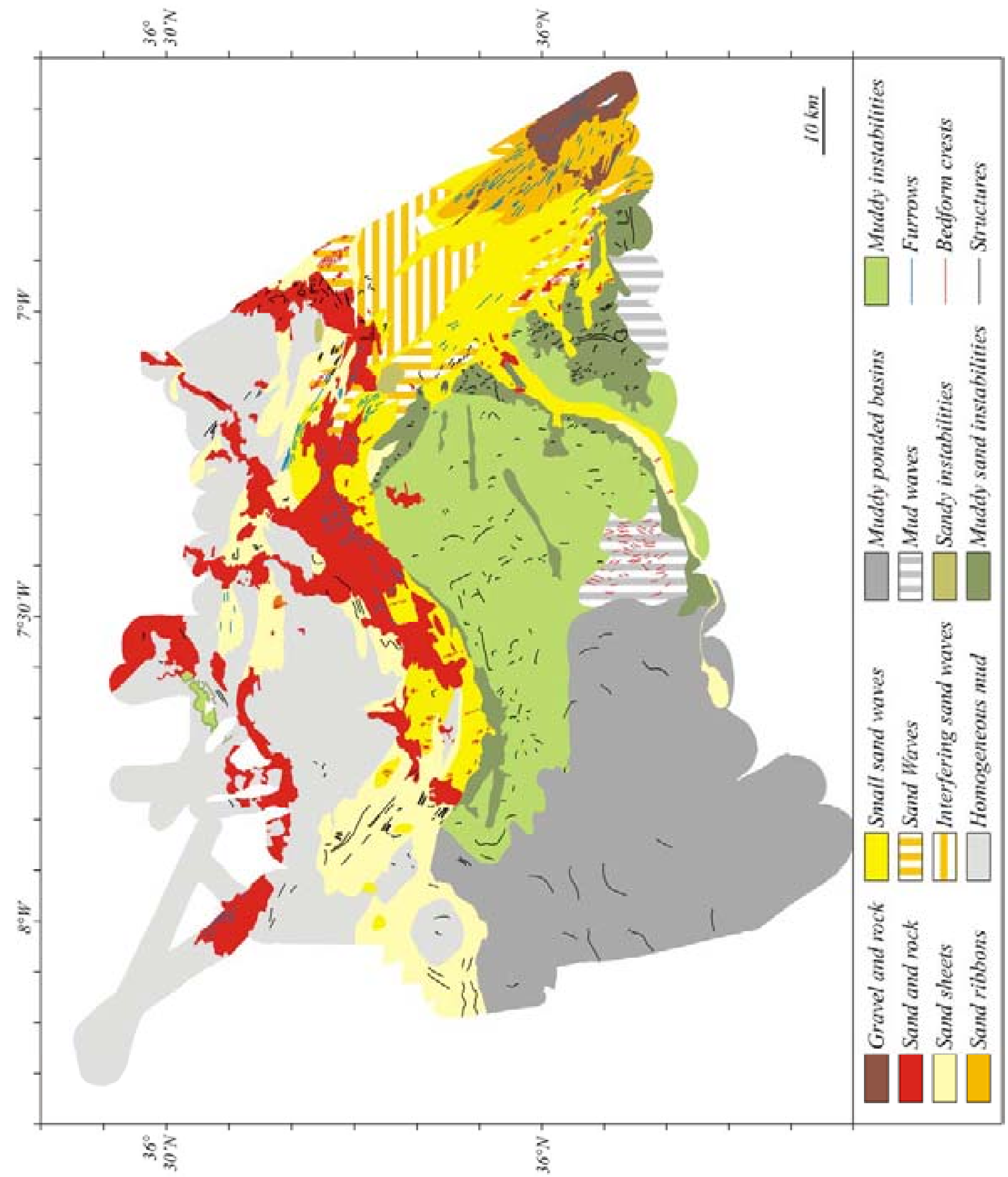
36° 30'N
36°N
7°W
7°30'W
8°W
10 km
Gravel and rock
Sand and rock
Sand sheets
Sand ribbons
Small sand waves
Sand Waves
Interfering sand waves
Homogeneous mud
Muddy ponded basins
Mud waves
Sandy instabilities
Muddy sand instabilities
Muddy instabilities
Furrows
Bedform crests
Structures

Figure 4

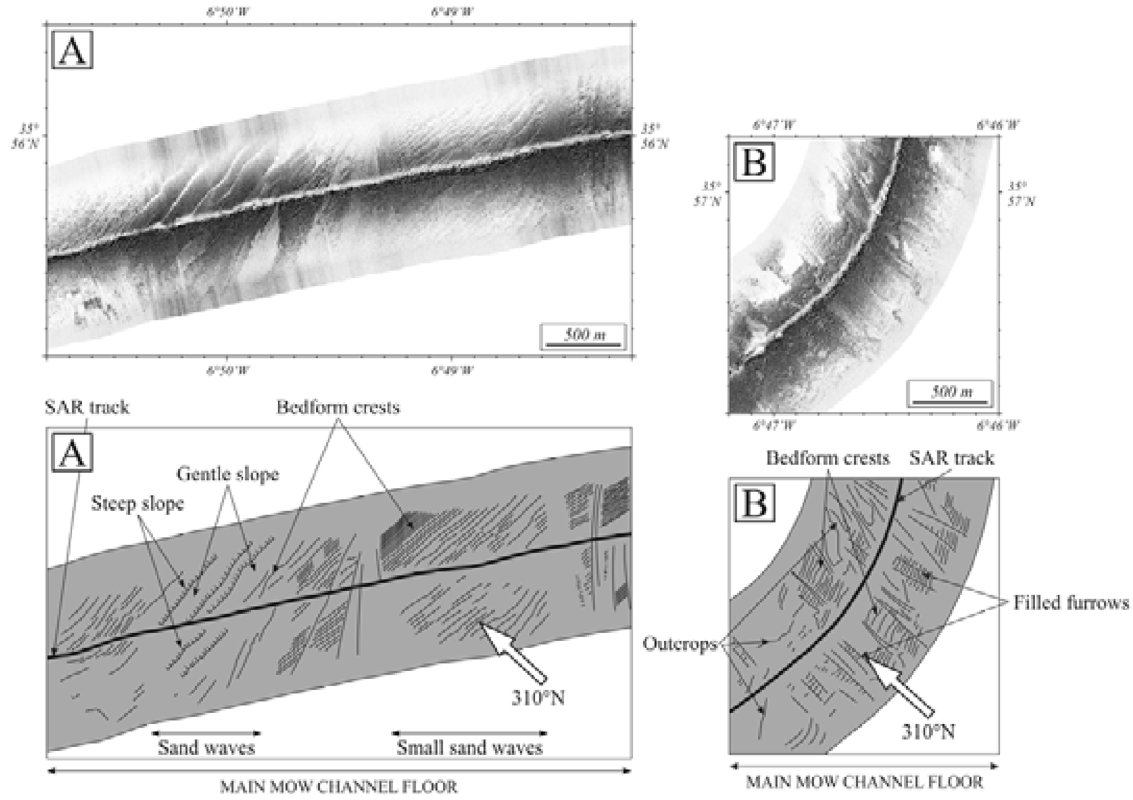

A
B
500 m
SAR track
Bedform crests
Gentle slope
Steep slope
310°N
Sand waves
Small sand waves
MAIN MOW CHANNEL FLOOR
Filled furrows
Outcrops

Figure 5

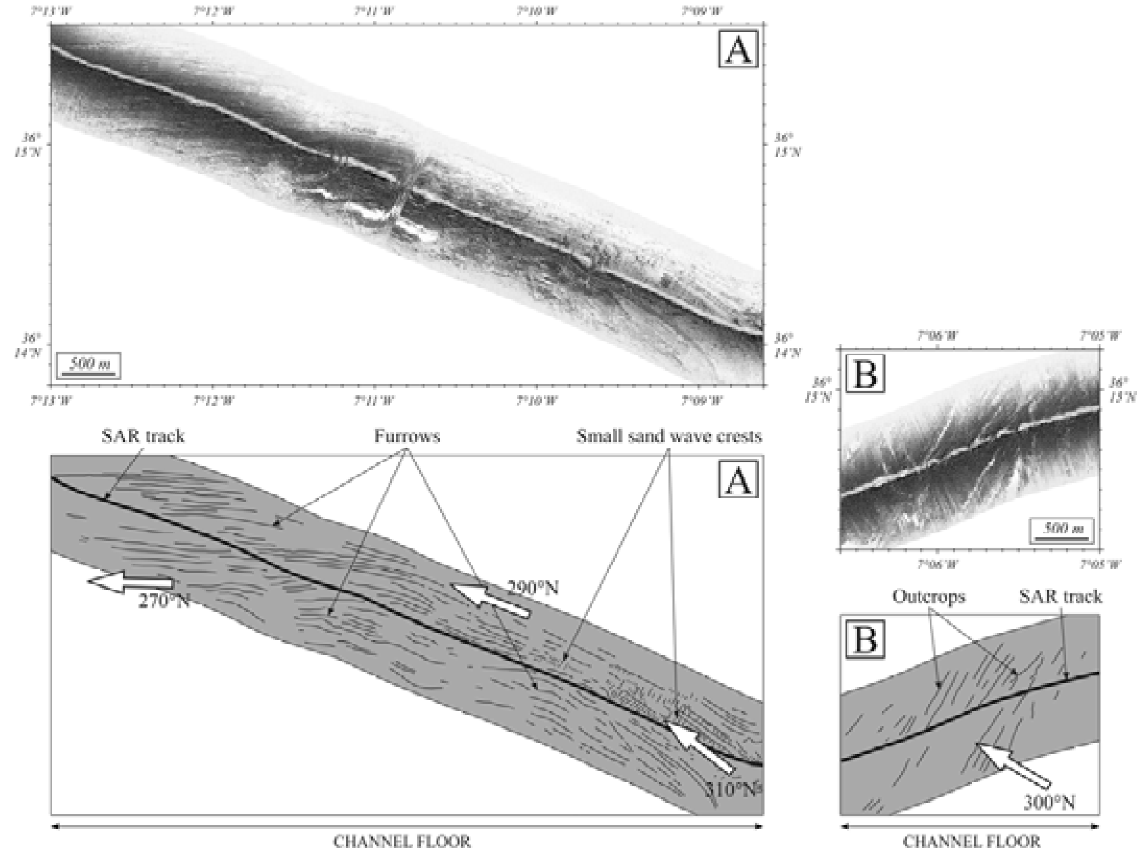
7°13'W
7°12'W
7°11'W
7°10'W
7°09'W
A
36° 15'N
36° 14'N
500 m
7°06'W
7°05'W
B
SAR track
Furrows
Small sand wave crests
290°N
270°N
310°N
CHANNEL FLOOR
Outcrops
300°N

Figure 6

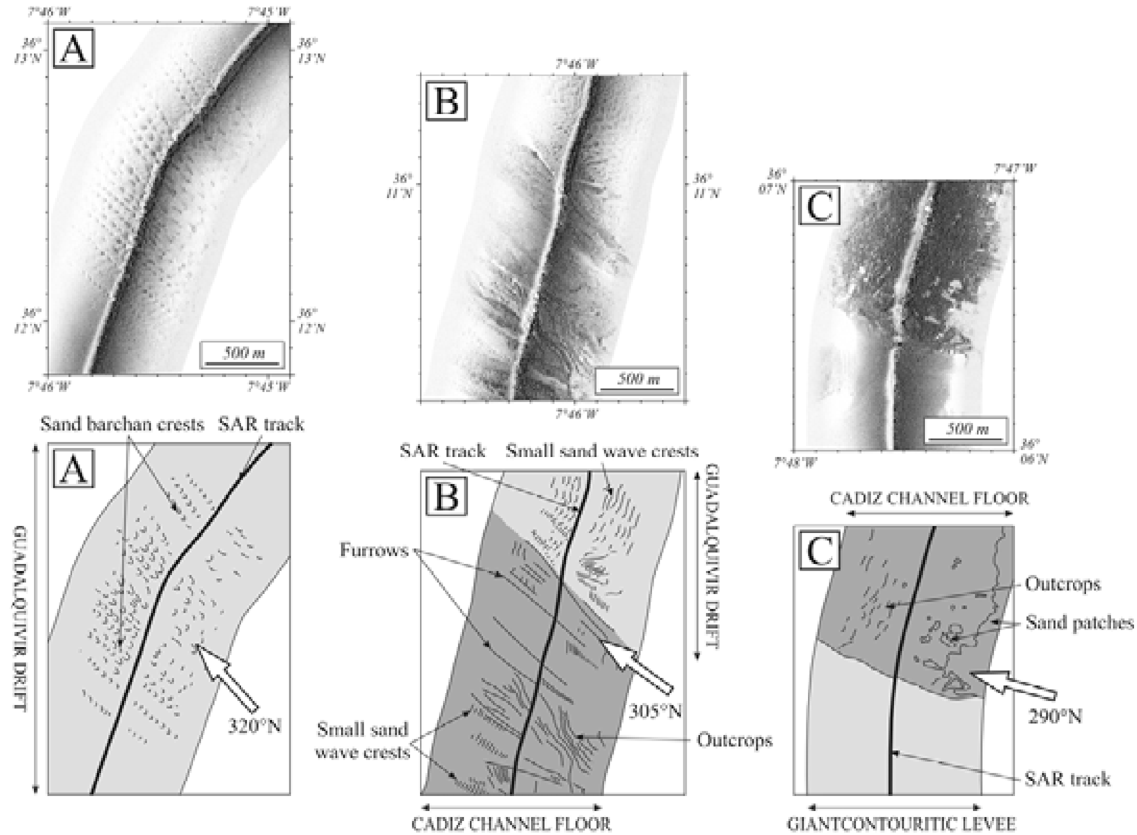

A
B
C
7°46'W
7°45'W
36° 13'N
36° 12'N
36° 11'N
36° 07'N
36° 06'N
7°47'W
7°48'W
500 m
Sand barchan crests
SAR track
GUADALQUIVIR DRIFT
320°N
Small sand wave crests
Furrows
305°N
Small sand wave crests
Outcrops
CADIZ CHANNEL FLOOR
Sand patches
290°N
GIANTCONTOURITIC LEVEE

Figure 7

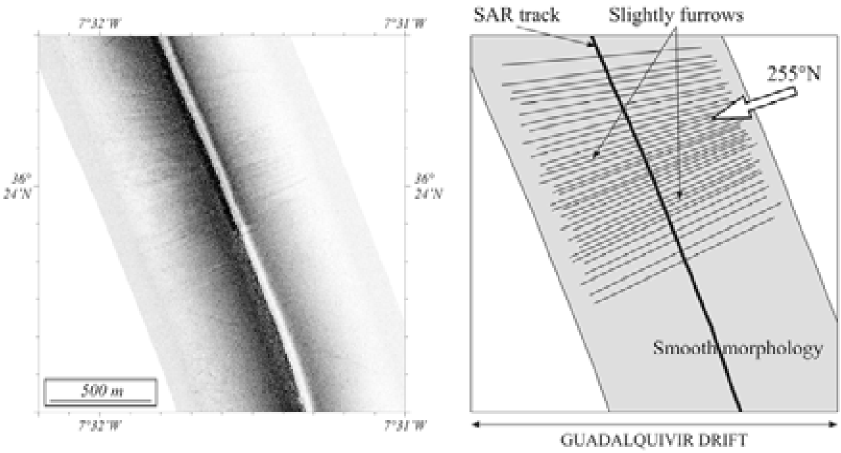

7°32'W
7°31'W
36° 24'N
500 m
SAR track
Slightly furrows
255°N
Smooth morphology
GUADALQUIVIR DRIFT

Figure 8

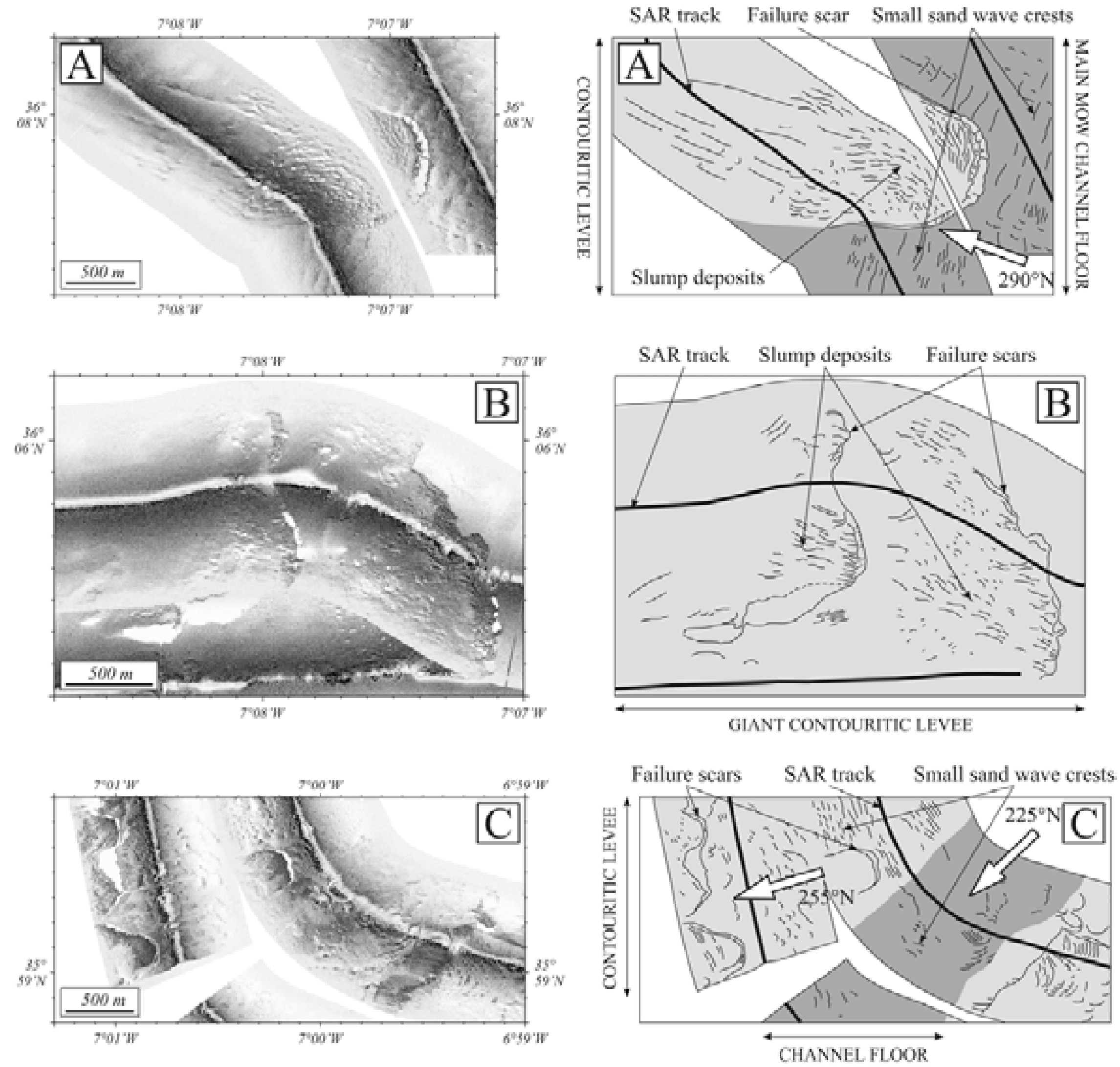

SAR track
Failure scar
Small sand wave crests
CONTOURITIC LEVEE
MAIN MOW CHANNEL FLOOR
Slump deposits
290°N
SAR track
Slump deposits
Failure scars
GIANT CONTOURITIC LEVEE
Failure scars
SAR track
Small sand wave crests
225°N
255°N
CONTOURITIC LEVEE
CHANNEL FLOOR
500 m

Figure 9

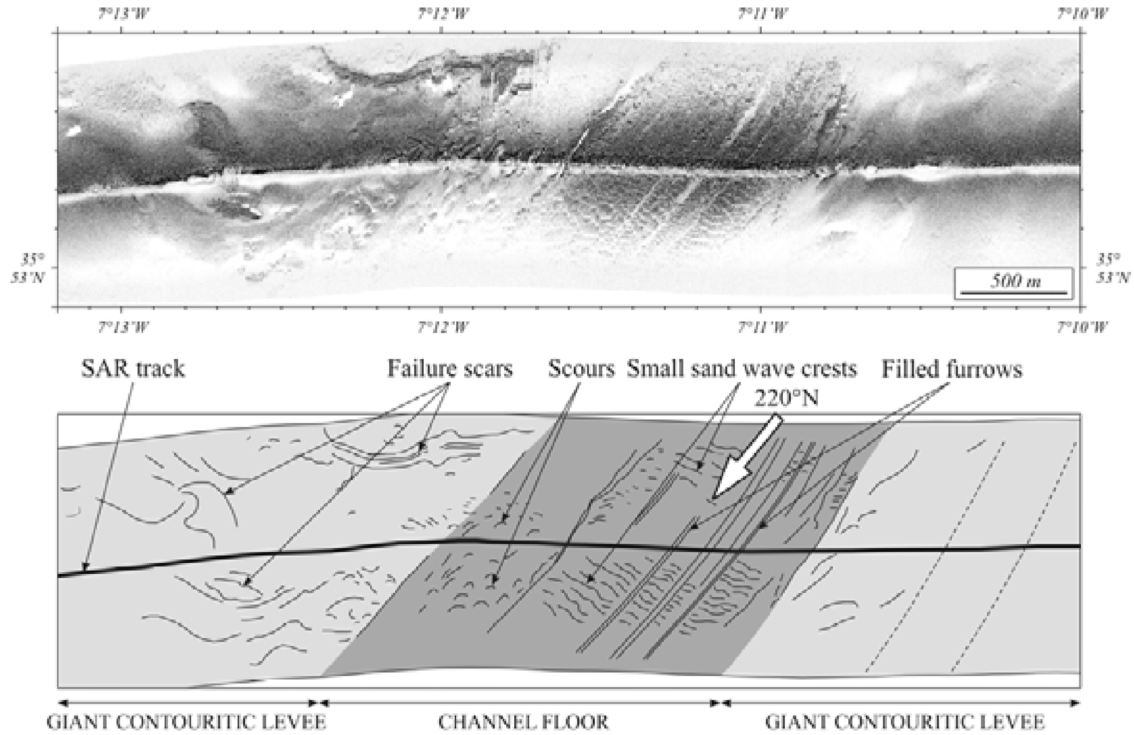
7°13'W
7°12'W
7°11'W
7°10'W
35° 53'N
500 m
SAR track
Failure scars
Scours
Small sand wave crests
220°N
Filled furrows
GIANT CONTOURITIC LEVEE
CHANNEL FLOOR
GIANT CONTOURITIC LEVEE

Figure 10

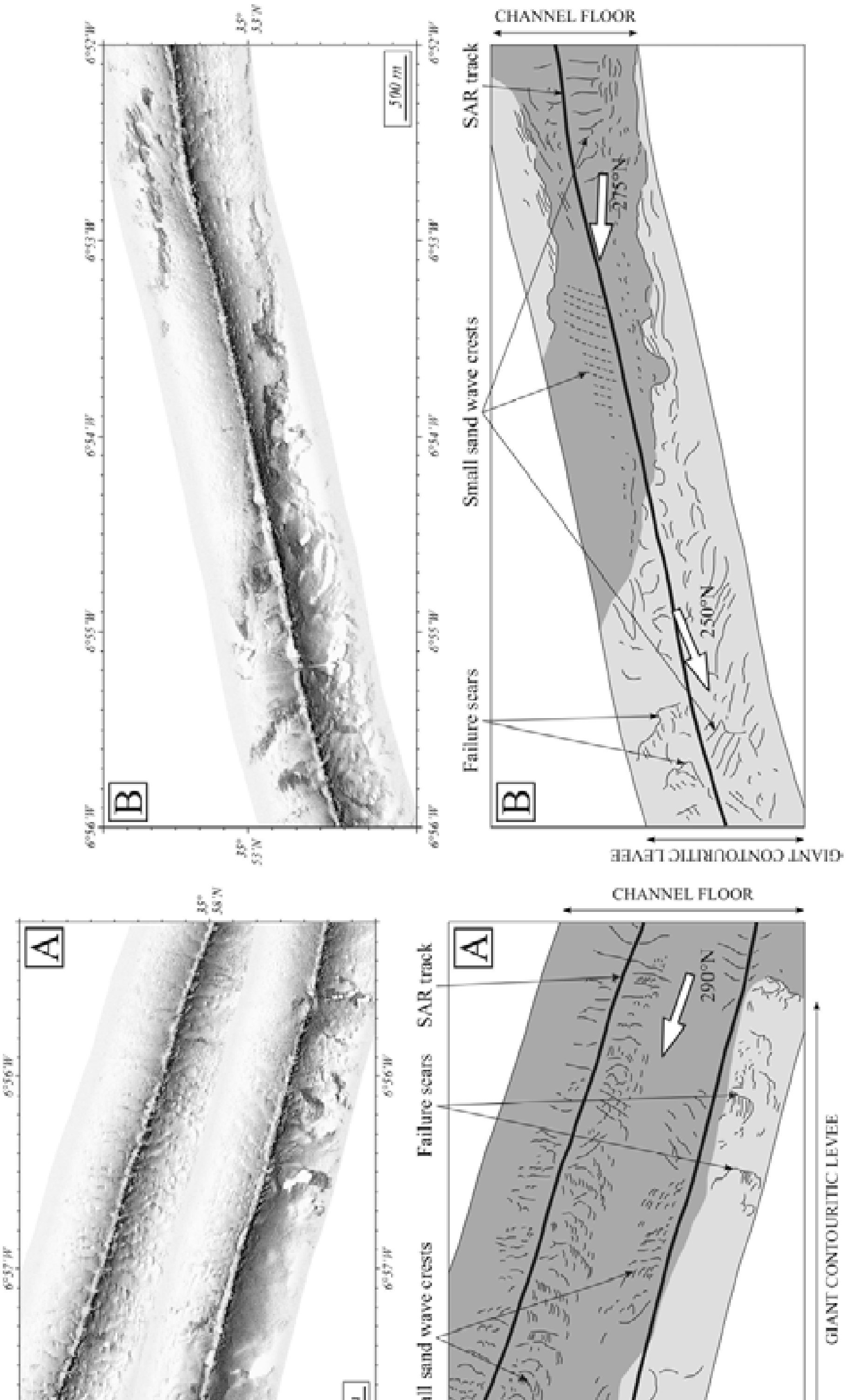

B
CHANNEL FLOOR
SAR track
Small sand wave crests
Failure scars
275°N
250°N
GIANT CONTOURITIC LEVEE
500 m
A
CHANNEL FLOOR
SAR track
Failure scars
Small sand wave crests
290°N
GIANT CONTOURITIC LEVEE
500 m

Figure 11

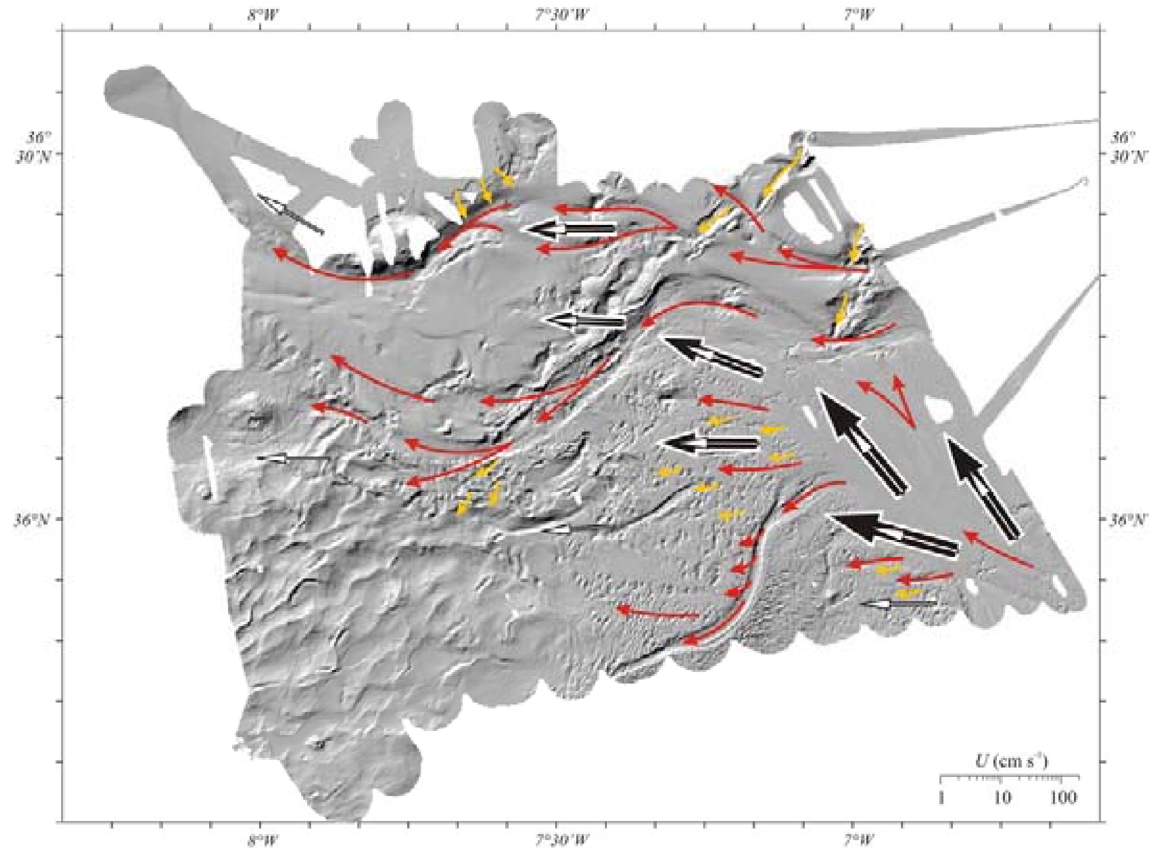

Figure 12

Core	Granulometric classes (%)			D90 (µm)	U^x (cm s^{-1})		U (cm s^{-1})	
	Clay (<10 µm)	Silt (10-63 µm)	Sand (> 63 µm)		Min.	Max.	Min.	Max.
CADKS01	4	9	87	627	1.80	10.5	32.0	190
CADKS02	3	8	89	395	1.60	6.50	28.0	115
CADKS03	2	3	95	659	1.90	11.0	34.0	200
CADKS04	31	59	11	64	0.95	*undefined* *	17.0	*undefined* *
CADKS05	34	61	5	46	0.85	*undefined* *	15.0	*undefined* *
CADKS06	35	61	3	38	0.80	*undefined* *	14.0	*undefined* *
CADKS08	6	17	77	211	1.30	2.80	23.0	50.0
CADKS09	8	23	69	271	1.40	4.00	25.0	70.0
CADKS11	9	33	58	191	1.20	2.00	21.0	36.0
CADKS14	30	53	17	101	1.00	*undefined* *	18.0	*undefined* *
CADKS15	6	25	69	150	1.10	1.50	20.0	27.0
CADKS18	20	39	41	189	1.20	2.00	21.0	36.0
CADKS19	16	34	50	550	1.70	9.50	30.0	170
CADKS20	23	57	20	136	1.10	1.30	20.0	23.0
CADKS22	39	52	9	57	0.90	*undefined* *	16.0	*undefined* *
CADKS23	31	63	6	44	0.85	*undefined* *	15.0	*undefined* *
CADKS24	37	62	2	33	0.80	*undefined* *	14.0	*undefined* *

* Fine-grained particles (D90<100 µm) are only transported as suspended load.

Table 1

Facies		EM300 imagery	SAR Imagery	Chirp profile	Facies		EM300 Imagery	SAR Imagery	Chirp profile
EROSION	*Rock and coarse sediments*		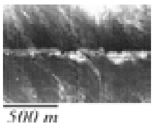	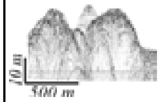	*DEPOSIT*	*Interfering sand waves*		*No data*	
DEPOSIT	*Sand sheets*	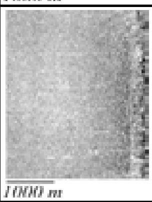	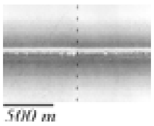			*Homogeneous mud*	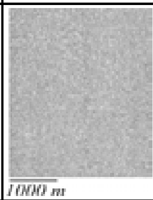	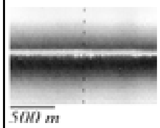	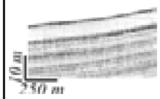
	Sand ribbons	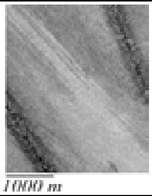	*No data*		*INSTABILITY*	*Mud waves*	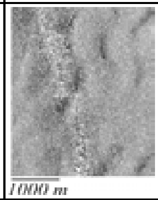	*No data*	
	Small sand waves		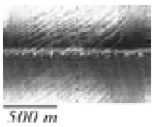	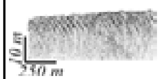		*Sandy instabilities*		*No data*	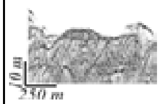
	Sand waves	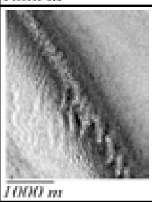	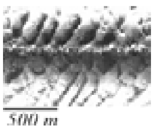	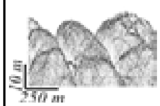		*Muddy instabilities*		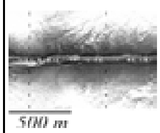	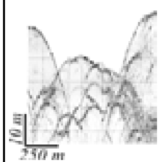

Table 2